The International Journal of Advanced Manufacturing Technology (2024) 131:4469–4482
https://doi.org/10.1007/s00170-024-13249-9

ORIGINAL ARTICLE

Pure niobium manufactured by Laser-Based Powder Bed Fusion: influence of process parameters and supports on as-built surface quality

Silvia Candela[1,2] · Pietro Rebesan[1] · Diego De Bortoli[3] · Simone Carmignato[3] · Filippo Zanini[3] · Valentina Candela[1,2] · Razvan Dima[1] · Adriano Pepato[1] · Markus Weinmann[4] · Paolo Bettini[2,5]

Received: 25 August 2023 / Accepted: 13 February 2024 / Published online: 26 February 2024

Abstract
Niobium (Nb) is a transition metal commonly used as an alloying element for increasing strength, toughness, corrosion resistance, and other properties of steel and superalloys. Pure Nb, however, is a very interesting metal for its excellent superconductivity. This makes it suitable for producing superconducting magnets and devices for particle acceleration systems and particle physics research (e.g., superconducting resonant cavities). In this work, the production of Nb by the Laser-Based Powder Bed Fusion (PBF-LB/M, also known as Laser Powder Bed Fusion or LPBF) process was examined. Manufacturing parameters were investigated to achieve additively manufactured parts with a relative density higher than 99.5% and showing a down-skin surface roughness in the range of 20–70 µm, depending on the inclination angle. Studies related to the limiting angle of self-supported Nb parts were also conducted, and innovative non-contact supporting structures were successfully developed. These allowed to creation of parts with very small overhang angles, without compromising the downward-facing surfaces; indeed at the same time, the as-built surface finish was improved.

Keywords Laser powder bed fusion · Niobium · Surface · Down-skin · Roughness

1 Introduction

Niobium was discovered by Charles Hatchett in 1801. Until 1844 and 1866, however, there was not a definitive distinction between niobium and tantalum: due to their similarities in chemical and physical properties, they are often found together in nature. In those 2 years, Heinrich Rose and Jean Charles Galissard de Marignac, respectively, demonstrated that two different elements exist [1, 2].

Like tungsten, molybdenum, and tantalum, niobium is one of the so-called refractory metals. The most peculiar properties of this special class of materials are high melting point (above the melting point of platinum, 2054 K), high-temperature strength and creep resistance, good corrosion resistance, and good thermal and electrical properties [3]. Niobium is especially appreciated because it is a superconductive material [3, 4]. A superconductor is defined as a material, or more generically a substance, that has zero electrical resistance below a well-defined critical temperature T_C, so it allows the transportation of electricity without any loss [3] and undergoes a reversible transition from the normal state to the superconducting one [5]. More precisely, niobium is a type II superconductor, which means that it has three different phases and two critical fields H_C: it switches from the Meissner state (superconducting state) to the Shubnikon phase, also called mixed or vortex state (for the particular structure that the type II superconductor has here), when the material is subjected to a magnetic field higher than the lower critical field H_{C1}. In this phase,

✉ Silvia Candela
silvia.candela@studenti.unipd.it

1 National Institute for Nuclear Physics (INFN) – Section of Padova, Via F. Marzolo, 8, 35131 Padova, Italy

2 Centro Ricerche Fusione (CRF), University of Padova, Corso Stati Uniti, 4, 35127 Padova, Italy

3 Department of Management and Engineering (DTG), University of Padova, Str.lla S. Nicola, 3, 36100 Vicenza, Italy

4 Taniobis GmbH, Im Schleeke 78-91, 38642 Goslar, Germany

5 Department of Industrial Engineering (DII), University of Padova, Via G. Gradenigo, 6/A, 35131 Padova, Italy

there is a partial penetration of the magnetic flux and the normal and superconductive phases co-exist. The material, then, crosses over to full flux penetration when the magnetic field is equal to or higher than H_{C2}, and behaves as a normal conductor [6].

Niobium and niobium-based materials are used for producing superconducting magnet systems of tokamaks [7, 8], but are also employed in the aerospace industry, electronics, and steel industry [3, 9–11]. Indeed, most of the world's produced niobium is used to create high-strength steel, because it acts as a grain refiner and a precipitation hardener in the alloy. Moreover, niobium enhances the corrosion resistance of steel [10].

Pure niobium is ductile, with respect to other refractory metals like tungsten (Table 1 summarizes the principal properties of niobium). Thus, it is not so difficult to process niobium via the more traditional subtractive mechanical methods. However, additive manufacturing (AM) allows for new perspectives in design and feedstock material usage optimization. This latter aspect can make the difference, especially if the raw material is a precious metal (so the wastage can be considerably reduced and minimized) or it is very expensive, as niobium is.

Depending on the nature of the precursor material (polymer, ceramic, metal) and its form (powder, wire, sheet), the AM technology that can be used differs. Laser-Based Powder Bed Fusion (PBF-LB/M, commonly named as Laser Powder Bed Fusion, LPBF) is an additive manufacturing technique specially developed for metals: a powder bed is selectively melted by a focused and high-power laser beam. The object is built up layer by layer. A thin layer of powder is spread onto a building platform by a coater blade, then an exposure phase follows, during which the laser scans the surface and melts the cross-section of the component that is under construction. After this, a new layer of powder is formed again and the cycle repeats. The process takes place in controlled conditions to prevent excessive oxidation of the metal or explosive reactions, in case a reactive material is used. Thus, the atmosphere inside the chamber is generally composed mostly of an inert gas (usually nitrogen or argon). The oxygen level is kept below 1%.

Table 1 Properties of pure niobium [1, 3]

Property	Value
Unit cell structure	Body-centered cubic (BCC)
Atomic number	41
Density [kg/m^3]	8570
Melting point [°C]	2468
Boiling point [°C]	4744
Elastic modulus [GPa]	110
Thermal conductivity [W/mK]	52.3 (measured at 20 °C)
Electrical resistivity [Ωm]	$144 \cdot 10^{-9}$ (measured at 25 °C)
Superconducting transition temperature [K]	9.2

With PBF-LB/M, it is possible to achieve almost fully dense parts, but many variables are involved in this kind of process, and all of them heavily influence the final quality of the material, both in terms of properties and surface topography. The poor as-built surface quality is often a huge limiting issue of AM [12, 13]. It is addicted to a wide number of factors that can be directly related to the process and the thermodynamic mechanisms that take place in the material [12]. The process parameters that greatly affect the surface quality are the following:

- Layer thickness and particle size: the more is thick the powder layer, the more is rough the surface of the additively manufactured part. The particle size distribution determines the height of the powder layer [14]: if the powder has many particles with small dimensions, the layer thickness should be small enough to guarantee the complete propagation of heat within the powder layer and the melting of all the particles of the powder bed, while if the particles are generally big, the layer thickness should not be too small; otherwise, only the smaller and fewer particles form the layer;
- Sloping/overhang angle: inclined surfaces are generally characterized by increased surface roughness, with respect to vertically or horizontally oriented walls. This is due to the fact that overhang areas are scanned over the powder rather than on solidified massive material. Together with the layer thickness parameter, it contributes to the so-called stair step effect (Fig. 1), which is the stepped approximation of the shape of the object due to the layer-by-layer manufacturing approach. This phenomenon is visible also on curved surfaces, not only on inclined ones [13–16];
- Surface parameters: laser parameters can be defined for the cross-section perimeter separately with respect to those for the inner areas. Contour and up-skin/down-skin parameters are defined for the external areas that are directly in contact with the powder. It is well known that the thermal conductivity of the powder is up to one hundred times lower than that of the same material in its bulky form because of voids between particles [17]. Thus, the cross-section perimeter is traced by a less

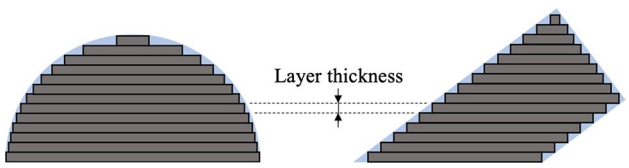

Fig. 1 Stair step effect

intense laser beam: in such a way, the amount of heat that is transferred to the metal does not propagate across a too-big volume within the powder, and surface dross formation is avoided;

- Use of supports: supporting structures are produced with the part in order to sustain its overhanging walls, giving it a "temporary" major stiffness during the building process and avoiding distortions due to the thermal stresses that could arise while printing, since supports allow a more effective heat dissipation. Supports are normally attached to the part, so the supported surface is inevitably compromised.

Some phenomena that might occur during the process also contribute to an increase in surface complexity and roughness: balling affects the roughness of the top surface of the part, while the sticking of partially molten particles to the boundaries of the melt pools inevitably worsens the surface finish of all the other surfaces [13, 18]. Even if the melt pool stability is low, the surface roughness increases: if the material does not have enough time to melt and wet the solid material underneath, the weld line forms with continuous interruptions and width fluctuations. Generally, surface treatments are performed as post-processing steps [13], but sometimes not all the surfaces are accessible by the etchants, the abrasives, or the mechanical tools, because of the complexity of the additively manufactured part geometry. Thus, improving as much as possible the as-built surface texture is sometimes compulsory.

The work here presented aimed at investigating the PBF-LB/M process of pure Nb: the main process parameters were intensively explored for maximizing the density of the additively manufactured parts, and for reducing the surface roughness. Much emphasis was put on the quality improvement of the downward-facing surfaces, which are characterized by defects such as dross formation and deformations [13]. Indeed, down-facing surfaces can represent a very challenging point for additive manufacturers, sometimes, because the poor heat exchange with the powder underneath can also affect seriously the geometrical accuracy of the whole part [19]. Also, the minimum self-supporting angle of pure Nb processed by PBF-LB/M was researched and several supporting structures were developed. The need of developing a new contact-less supporting system was dictated by the necessity of obtaining a good as-built surface finish also on the downward-facing surfaces characterized by a very low overhang angle, in order to achieve a much more homogeneous surface roughness of the pieces produced via PBF-LB/M. In the literature are reported some interesting studies concerning the use of contact-free structures as heat sinks and supporting parts using different metallic materials [13, 19]; thus with this work, the efficacy of such a kind of support for the PBF-LB/M process of pure niobium was assessed.

2 Materials and methods

The gas-atomized pure niobium powder AMtrinsic® Spherical Nb produced by Taniobis GmbH (Goslar, Germany) was used in this experience. The powder had a particle size distribution (PSD) ranging from 20 to 60 µm (D10=14.23 µm, D50=32.16 µm, D90=56.79 µm). A PSD graph of the powder is reported in Fig. 2. The flowability was measured

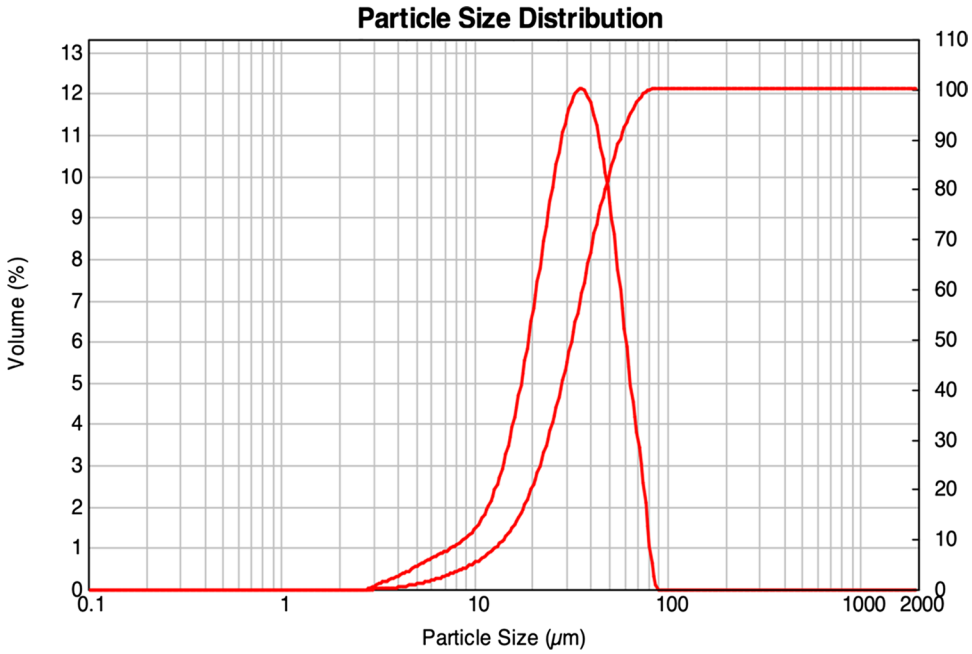

Fig. 2 Particle Size Distribution map of the powder

using a Hall Flowmeter by the producer. The test revealed a Hall Flow of 17 s (0.1') and 4 s (0.2'). The tap density was 5.2 g/cm^3.

A morphology examination of the powder particles was performed using a Zeiss Sigma HD Scanning Electron Microscope (SEM), (Zeiss Group, Oberkochen, Germany). Figure 3 shows some images of the powder, taken at different magnifications. Table 2 then reports the chemical composition of the powder used. As can be seen from Fig. 3, the powder is mostly spherical, but small particles' agglomerates and satellites are also present. Few particles show an irregular shape. However, the spherical degree of the powder used is quite good. The flowability of the powder is a key factor for a good PBF-LB/M process because if the particles flow easily, the powder bed is homogeneous. Thus, the powder layer is properly formed, and the quality of the printed parts improves.

In this work, an EOS M100 DMLS (Electro-Optical Systems GmbH, Krailling, Germany) was employed. This machine is equipped with a Yb:YAG fiber laser having a nominal power of 200 W and a wavelength of 1064 nm. The laser spot has a diameter of 40 µm. The building area is a circle with a diameter of 100 mm, while the maximum height that can be reached is 95 mm. The process took place in a controlled atmosphere: argon was used as inert gas for filling the process chamber and the oxygen content was kept below 0.1% during the printing. The building platform was not pre-heated.

Table 2 Composition of the powder [20]

Element	Quantity [ppm]
Nb	99.9%
C	<50
H	<50
N	<100
O	<600
Ta	<100
Cr	<50
Fe	<50
Ni	<50
Hf	<50
Mo	<50
Zr	<50
W	<50

2.1 Density and Single Scan Tracks analysis

An intense process parameters fine-tuning campaign was performed as the initial step of the research on PBF-LB/M of pure niobium, in order to find a process parameters set that allows obtaining a relative density higher than 99.5%. Several samples were produced with different combinations of laser power, scanning speed, and hatch distance. The power was set in the range of 100–160 W, while the scanning velocity and the hatch spacing values from 250 and 550 mm/s and 0.04–0.06 mm were used, respectively. For all the samples produced, the scanning strategy was the same: a stripes pattern was used, setting the stripes width to 5 mm and the stripes overlap to 0.05 mm, while the scanning rotation angle of 67° was applied between adjacent layers. The layer thickness used in this work was 30 µm. Also, the influence of the scanning strategy on the final density of the parts was investigated by reducing the stripes width to 3 mm. The parts were printed onto a building platform made of copper OFE (Oxygen Free Electrolytic). This choice was dictated by the authors' experience with other refractory metals [21]: it is known that stainless steel substrates are not suitable for refractory metals because brittle intermetallic phases form at the interface between additive manufactured parts and the platform, or more in general, in the weld zone, so the adhesion to the building substrate is poor and the job failure due to the detachment of the parts under construction is highly likely. As reported by Hajitabar et al. [22], niobium behaves in the same manner as molybdenum and tantalum, for example [21, 23].

Cubic samples were produced with different dimensions: a first trial was performed for evaluating a wider range of laser power values, so the dimensions of the cubes were 7 mm × 7 mm × 7 mm, due to the limited building area.

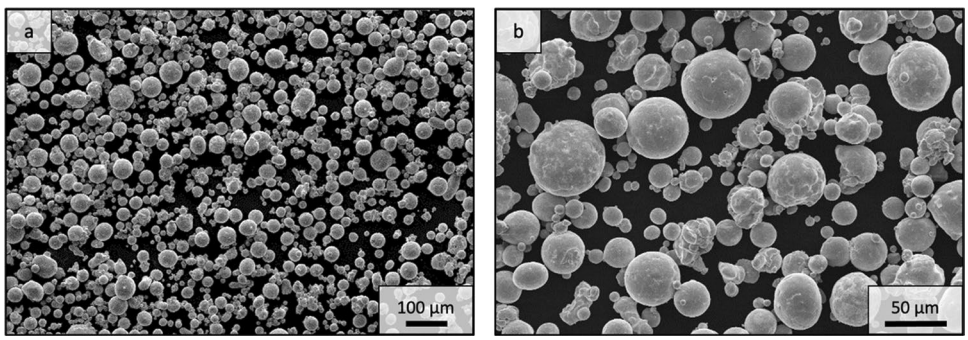

Fig. 3 SEM images of the AMtrinsic® Spherical Nb powder: **a** magnification ×100; **b** magnification ×300

Relative densities were measured with the Archimedes method, while the top surfaces of the samples with the higher densities were also examined with SEM.

Trials were performed to investigate the influence of scanning speed, laser power, and hatch spacing on the density and find out the optimum process window, basing the choice of the parameters on the volume energy density E_V. It can be estimated according to Eq. (1) [24]:

$$E_V = \frac{P}{s \bullet h \bullet t} \tag{1}$$

where P is the laser power [W], s is the scanning speed [mm/s], h is the hatch spacing [mm], and t is the layer thickness [mm]. In particular, the combinations of parameters were selected in order to cover a wide range of energy densities. The cubes' dimensions were increased to 10 mm × 10 mm × 10 mm once the optimal power and the velocity of the laser were detected. In the end, two samples were produced adopting the remelting strategy: for one of them, the first exposure was higher in energy with respect to the second, while for the other sample, the exposure types were the same, but the order was inverted.

Single scan tracks (SSTs) were also produced for evaluating the quality of the melt pools created by the different parameters sets used for printing the cubes. SEM images were taken for each SST in order to evaluate the homogeneity of the single melt pool, then the ImageJ software was employed for measuring the widths.

2.2 Contour parameters

Contour parameters were also examined, and dimensional verifications were performed on specially designed samples. Ten hollow cubic samples were produced, with a wall thickness of 1 mm, a side of 10 mm, and a height of 8 mm (Fig. 4a). In this test, two contours were applied for each sample. The laser power was kept constant and equal to 110 W, while the scanning speed and the offset parameters varied. The geometrical accuracy was then assessed by using a Zeiss Accura MASS (Zeiss, Oberkochen, Germany) coordinate measuring machine (CMM). A tungsten carbide probe with a diameter of 2 mm was used. The dimensional control was crucial for the further steps of this study, especially for the development of the contactless supporting structures that will be described in the next paragraph. Table 3 summarizes the contour parameters that have been tested. In Fig. 4b are shown the paths of the measurement probe on each sample: 3 different height levels were considered (2 mm, 4 mm, and 6 mm from the platform plane). The integrity of the contour was verified by printing other cubes and acquiring the morphology of the surfaces with a Sensofar S Neox optical profilometer (Sensofar, Barcelona, Spain) since, in previous experiences, the authors observed that the gas flow and the recoater may cause a discontinuity of the contour, especially on the faces on the opposite side with respect to the two different directions, and a comparison of the as-built surface roughness of samples with and without contour was also done.

The instrument was used in the *focus variation* modality with a 20× objective to scan the surfaces of interest

Table 3 Contour parameters tested

Sample	Power [W]	Speed [mm/s]	Part offset [mm]	Offset 1 [mm]	Offset 2 [mm]
1	110	275	0.16	0.04	0.06
2	110	250	0.16	0.04	0.06
3	110	225	0.16	0.04	0.06
4	110	200	0.16	0.04	0.06
5	110	175	0.16	0.04	0.06
6	110	275	0.16	0.05	0.05
7	110	250	0.16	0.05	0.05
8	110	225	0.16	0.05	0.05
9	110	200	0.16	0.05	0.05
10	110	175	0.16	0.05	0.05

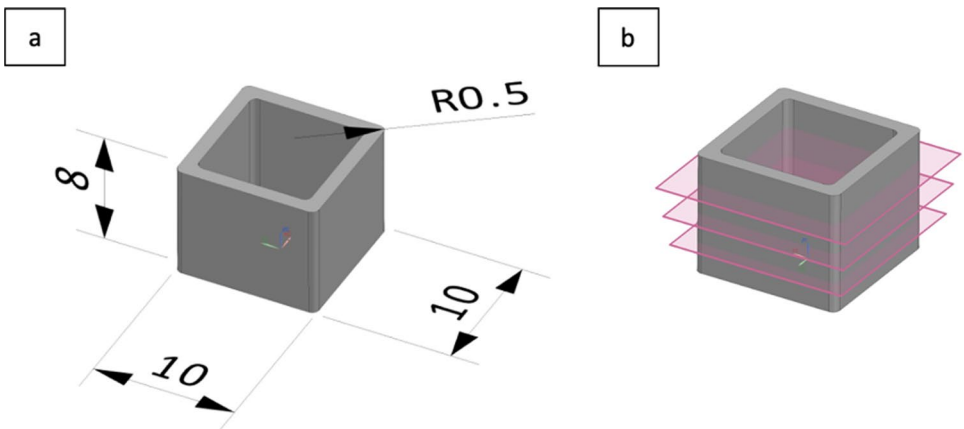

Fig. 4 Samples for the study of the contour parameters: **a** sample dimensions; **b** heights at which the samples were analyzed

and reconstruct their three-dimensional topography. The acquired data were elaborated in accordance with ISO 25178-2 [25] to compute the *Sa* areal surface texture parameter, which represents the average absolute ordinate value of the scale-limited surface. In particular, *Sa* was computed on the S-F surfaces, applying an F-operator based on the least-squares plane to remove the form error, and an S-filter with a cut-off λs equal to 2.5 µm to reduce the instrument noise.

2.3 Overhanging angles, down-skin parameters and supports

In the PBF-LB/M process, the overhang surfaces that have a critical slope need to be held up by removable structures. This critical angle is influenced by the material (e.g., its thermal properties, the characteristics of the powder), the machine, and the process parameters. In general, supports are produced for those surfaces having overhanging angles lower than 45°. However, the use of traditional supports implies that these surfaces show connection marks once the supports are removed. In this study, the minimum overhanging angle for niobium was researched. Once the fine-tuning of the process parameters has been completed for the core, the attention was focused on the down-skin parameters in order to investigate the minimum self-supporting angle of AM pure Nb. For this test, segmented arcs like that represented in Fig. 5 were printed, with overhanging angles varying in the range of 20–45° by a step of 5°. The samples had a thickness of 2 mm to ensure stiffness, and the down-skin surfaces had an area of 3 mm × 6 mm to perform measurements. Different down-skin parameters were assigned to the samples, and the downward-facing surfaces were then analyzed with the optical profilometer Sensofar S Neox to understand the influence of process parameters on the surface roughness.

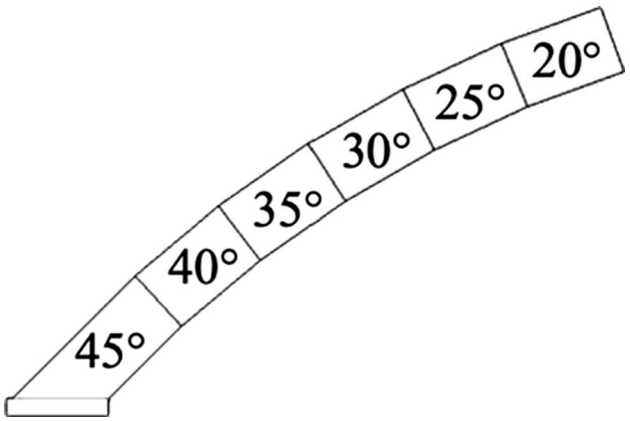

Fig. 5 Segmented arc for determination of niobium limiting critical angle. The inclination angles reported in the picture refer to the angles between the surface plane and the horizontal direction

Subsequently, the same kind of sample was used for evaluating the effectiveness of contact-free supporting structures. This novel supporting system was designed as reported in Fig. 6. Traditional block supports were also employed, in order to reduce the amount of material used in the job. For simplicity, from now on the parts composing this supporting system will be named simply as "supports," as reported in the scheme of Fig. 6. The supports were placed under the arcs to cover the entire downward-facing areas. The down-skin parameters were kept constant for all the samples, while the gap between the part and support ranged between 3 and 7 times the layer thickness: 90 µm, 150 µm, and 210 µm. Then, the down-skin surface roughness was measured for evaluating the effectiveness of such innovative supporting structures and establishing the minimum gap value that allows the pieces not to stick and heat to be dissipated properly.

3 Results and discussion

3.1 Density and Single Scan Tracks analysis

As previously mentioned, the relative density of the cubic samples obtained with different parameters combinations was assessed with the Archimedes method, by measuring first the weight of the parts in air, and then dipping them in distilled water. The formula utilized to obtain the apparent density of each additively manufactured sample is the following [26]:

$$\rho_{AM\ Nb} = \frac{m_{dry}}{m_{dry} - m_{wet}} \bullet \left(\rho_{water} - c\right) + c \tag{2}$$

where m_{dry} is the weight of each cube in air, m_{wet} is the weight measured in water, ρ_{water} is the density of water as a function of the temperature at which the measurement is performed, and c is a corrective factor of air, that is equal to

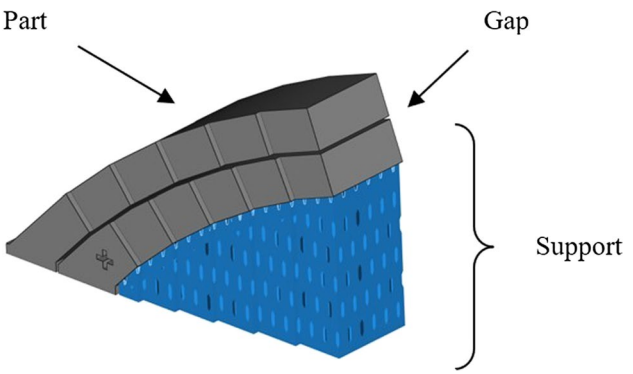

Fig. 6 Representative design of samples with contactless supporting structure

0.0012 g/cm^3. The relative density of AMed niobium is then calculated as follows:

$$\rho_{\%} = \frac{\rho_{AM\ Nb}}{\rho_{bulk\ Nb}} \bullet 100 \quad (3)$$

where $\rho_{AM\ Nb}$ is the apparent density computed using Eq. (2), and $\rho_{bulk\ Nb}$ is the density of wrought niobium.

The instrument that was used is a Mettler-Toledo ME balance (Mettler-Toledo GmbH, Greifensee, Switzerland). The reference density of wrought niobium was fixed at 8.57 g/cm^3 [2, 3]. The densities obtained ranged from 98.17 to 99.87%.

Laser power had the most visible effect on the melting quality during the PBF-LB/M process: the specimens built using the highest power values saw a marked balling effect during the building process. Good quality of the top surface was achieved for those samples manufactured with a laser power equal to 110 W or slightly lower/upper, since the absence of balling or spatters formation was noticed. However, the maximum density was observed for only the cube produced with a power of 115 W. The effect of scanning velocity was less significant. In general, both the hatching distance values tested (0.04 mm and 0.06 mm) were good, because the adjacent melt pools overlapped properly, without leaving Lack of Fusion (LOF) defects in-between or, on the contrary, re-fuse excessively the material of the previous melt pool. Figure 7 shows the top surfaces of several samples printed. It is possible to see that a scanning speed equal to 300 mm/s (Fig. 7b) can be considered adequate for niobium, because the melt pools are more regular, while 500 mm/s (Fig. 7a) is a barely acceptable value: the edges of the melt pools are more irregular; thus, the molten pool is unstable with such a velocity.

The samples produced using a smaller stripes width (3 mm) were slightly less dense if compared to the samples produced with the same laser parameters but wider stripes (5 mm), even if the difference was not appreciable, while for the cubes that saw a remelting, it was noticed that the exposure order can also have a little effect on the final properties of the parts. Indeed, the sample produced using first the more powerful exposure had a relative density 0.57% higher with respect to the other cube. However, the authors do not consider the remelting strategy valid for justifying the increase in time that it inevitably leads to. In Table 4, the relative densities, computed using Eq. (2) and Eq. (3), are reported in relation to the printing parameters used for some of the samples produced.

Single Scan Tracks (SSTs) were also produced to see the quality of the melt pools created by using the same exposure

Table 4 PBF-LB/M parameters used and relative densities obtained for pure niobium samples

Power [W]	Scanning speed [mm/s]	Hatch spacing [mm]	Stripe width [mm]	Relative density [%]
100	450	0.04	5	91.57
105	300	0.04	5	99.78
110	275	0.04	5	99.15
110	300	0.04	5	99.57
110	300	0.06	5	99.17
110	325	0.04	5	99.69
115	300	0.04	5	99.87
120	300	0.04	5	98.95
120	300	0.04	3	98.23
130	300	0.04	5	98.91
130	300	0.04	3	98.49
130	300	0.06	5	98.95
130	300	0.06	3	98.68
160	350	0.06	5	97.98
140 90	300	0.04	5	99.34
90 140	300	0.04	5	98.77

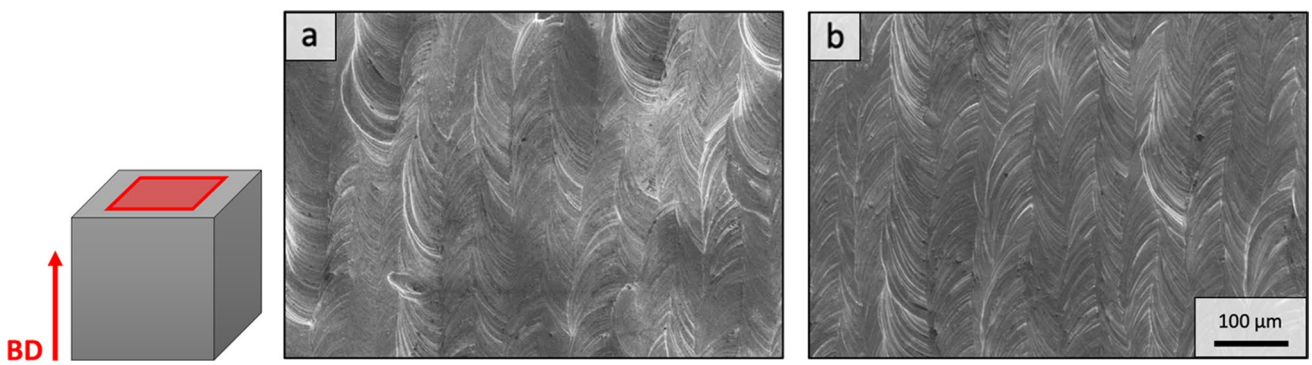

Fig. 7 Representation of the scanned areas and top surfaces of some samples printed with different parameters: **a** P= 110 W, v= 500 mm/s; **b** P= 120 W, v= 300 mm/s. A slower velocity allows to have more stable melt pools

parameters of the cubes. The average width, continuity, and homogeneity of the scan tracks were examined. Figure 8 shows the SEM images of the SSTs examined in this work. From this test, it can be seen that a scanning speed higher than 350 mm/s is too elevated independently from the laser power that is employed, and the melt pool appears continuously interrupted because the material did not have enough time to melt completely. Indeed, it is evident that many powder particles are stuck on the edges of these melt pools, while partially melted particles are less numerous on the melt pools generated using lower laser speeds. High power and low velocity combined together are more prone to generate a wider melt pool. This means that the energy supplied to the material is tendentially elevated. In general, the SSTs obtained are mostly homogeneous and there are not-so-evident balling phenomena. The ImageJ software was employed for estimating the width of the single scan tracks. The average widths of the several single scan tracks are plotted in Fig. 9 as a function of laser power and scanning speed. As can be clearly noticed from Fig. 9, a lower scanning speed generates a wider SST, independently from the power employed.

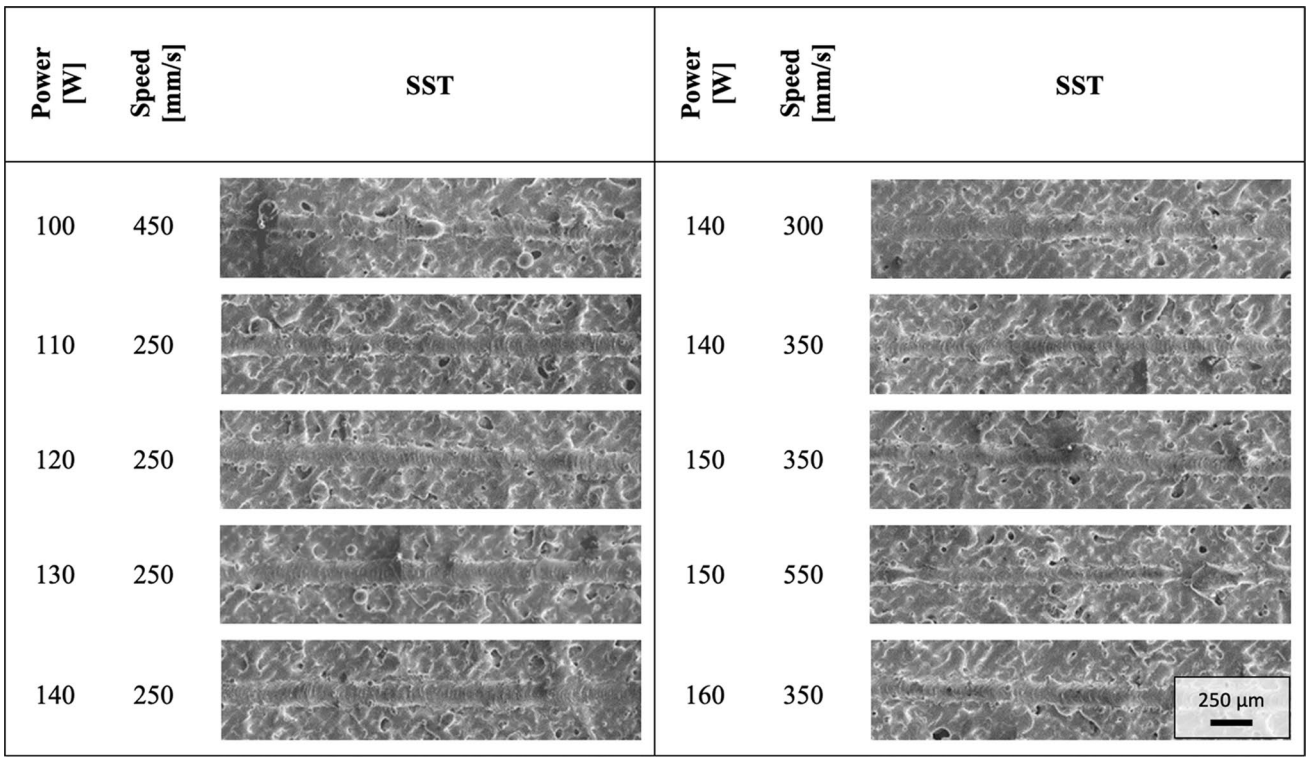

Fig. 8 Single scan tracks (SSTs) obtained with different laser exposure parameters

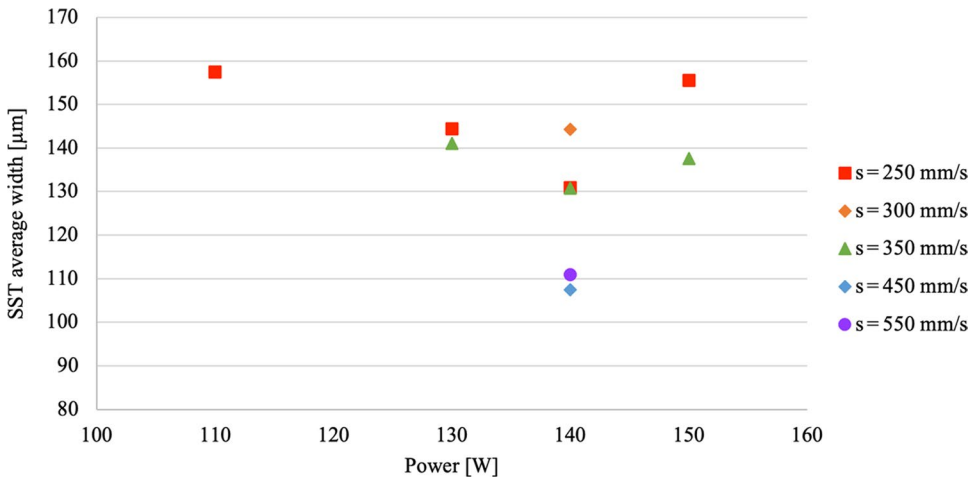

Fig. 9 Average width of the single scan tracks printed with different laser power and scanning speed

3.2 Contour parameters

As previously described, the geometrical accuracy of the samples produced was measured at three different heights with a Zeiss Accura CMM machine. This analysis gave preliminary information about the surface quality of the samples. As can be seen from Fig. 10, peaks on the surfaces were detected by the probe. Unfortunately, in all the samples, the contour revealed to be not uniform, and discontinuities were present, especially on the surface of the sample oriented on the opposite side with respect to the gas flow direction. The recoater seemed to contribute to "break" the contour, too, because the peaks were often much higher in the corners where the first contact between the blade and the part occurs (for major clarification, the upper image of Fig. 10 shows the position of the samples onto the platform).

In Table 5, the average values of the displacements acquired with the CMM with respect to the CAD dimensions of the parts are reported. From the test, sample 4 and sample 5 had the most homogeneous surfaces: the contour had much fewer discontinuities with respect to the other samples. Probably, this is due to the central position of samples 4 and 5 on the platform. Samples 7 and 8, however, showed to have a constant average displacement from the CAD dimensions on the three paths considered, though the surfaces had numerous burrs and irregularities.

Cubic samples were then printed defining the contour and were also analyzed with an optical profilometer to measure the as-built surface roughness on the vertical faces of the cubes. The three-dimensional surface topography acquisition and *Sa* computation were performed as described in Section 2.2. Also here, the surfaces on the opposite side of the gas flow were remarkably rougher with respect to the other sides of the cubes. As previously mentioned, the gas flow might be directly involved in this phenomenon: it is possible that, if the gas flow is vigorous, the contour scan track faces discontinuities or irregularities that may be caused by the local accumulation of the by-products of the process on the laser path. The non-uniform amount of material that must be melted along the track can surely affect the melt pool stability and determines a higher surface roughness. Though, further investigations need to be done to better understand the role of the gas flow on the contour quality. From the measurement, however, it was noticed that the contour helped decrease the roughness of the parts, except for the surfaces indicated above: from a *Sa* higher than 22 µm measured on the vertical surfaces of samples without contour, the cubes for which the contour was defined had an as-built *Sa* of 10 µm. Figure 11 shows a qualitative comparison of the as-built surface topography of samples obtained with and without using contours. The vertical surface of the sample produced without contour is visibly more complex and less homogeneous than the surface obtained with contour.

3.3 Overhanging angles, down-skin parameters and supports

In a first step, samples like that represented in Fig. 5 were produced without any kind of support for evaluating the minimum self-supporting angle, or critical angle, of niobium parts produced with PBF-LB/M. The same core laser parameters were used for all the arcs, while different down-skin parameters were defined, in order to find out the more appropriate combination of laser power and scanning speed. Laser power included between 55 and 70 W and scanning speeds ranging from 450 and 550 mm/s were tested. The down-skin overlap was set equal to 6 µm. As previously mentioned, downward-facing surfaces are generally the worse in terms of as-built surface finish and geometrical accuracy because heat dissipation is strongly hampered by the underlying powder, so the development of a specific set of down-skin parameters would help reduce the energy supplied to the material and so the overheating is avoided [19]. At the same time, the melt pool is smaller than that of the outer skin ones.

The critical angle is defined as the minimum angle between the inclined downward-facing surface and the building platform plane at which the use of supporting structures can be avoided. It depends on the material, of course, but also on the process parameters [17], in terms of energy supplied by the thermal source. When the building process is taking place, the smaller the inclined angle of the downward surface, the harder the heat dissipation. Because of this, warping may occur, and edges of the part may start arising layer after layer. If this happens, the powder layer will not have a homogeneous thickness across the building area because the recoater starts jumping (see Fig. 12) and, in the worst case, the job fails after the collision of the blade on the warped part under construction.

It was found that the critical angle of niobium lies between 20 and 25°. The down-skin parameters with which overheating was limited only for angles lower than 25° are 70 W of power and a scanning velocity of 450 mm/s. However, for angles lower than 30°, the surface still appeared with dross formation and irregularities.

The use of contactless supports allowed for reaching smaller angles and, in some cases, completing the formation of the arc. It was noticed that the down-skin parameters and the gap work synergically. So, it is extremely important to experiment with both two variables at the same time for optimizing as much as possible the production of inclined surfaces by using contact-free supporting structures. Indeed, it was seen that using a scanning velocity of 450 mm/s for the down-skin, the parts were in general characterized by a lower as-built surface roughness with respect to those obtained with a slightly higher speed (500 mm/s, lines with square marks in the graph). The parts that went

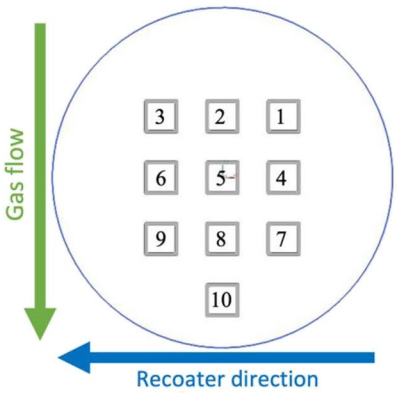

Sample 3

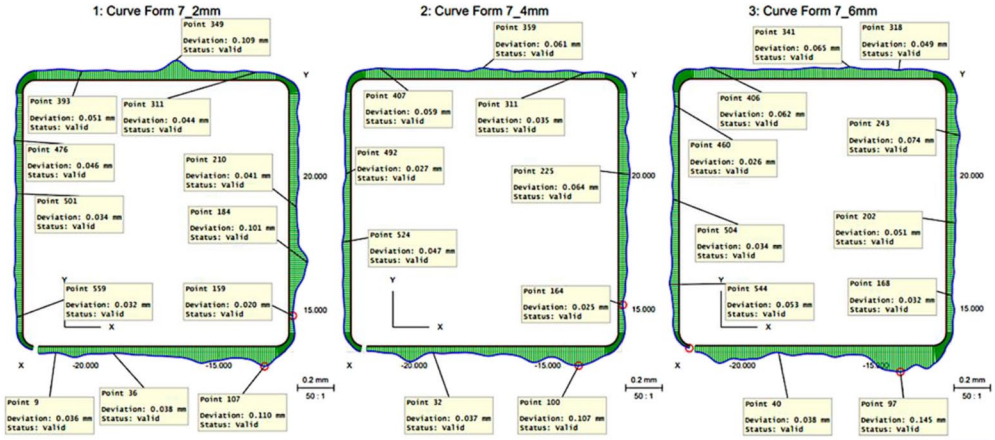

Sample 4

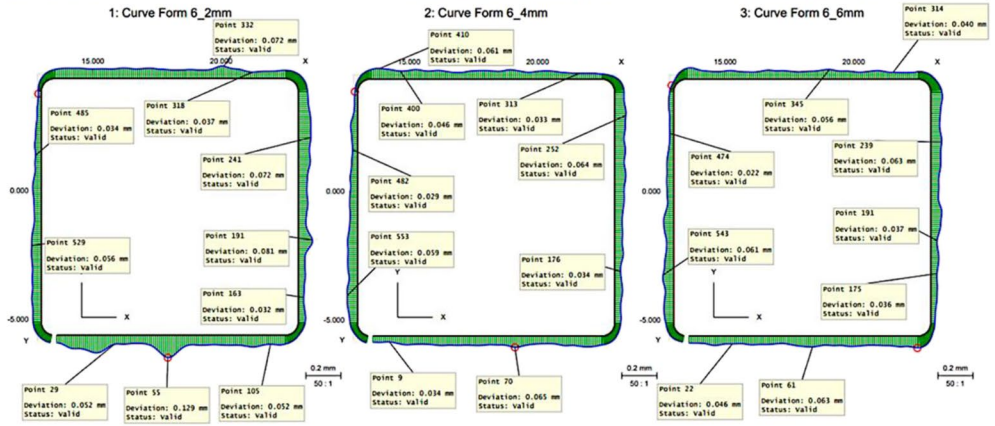

Sample 8

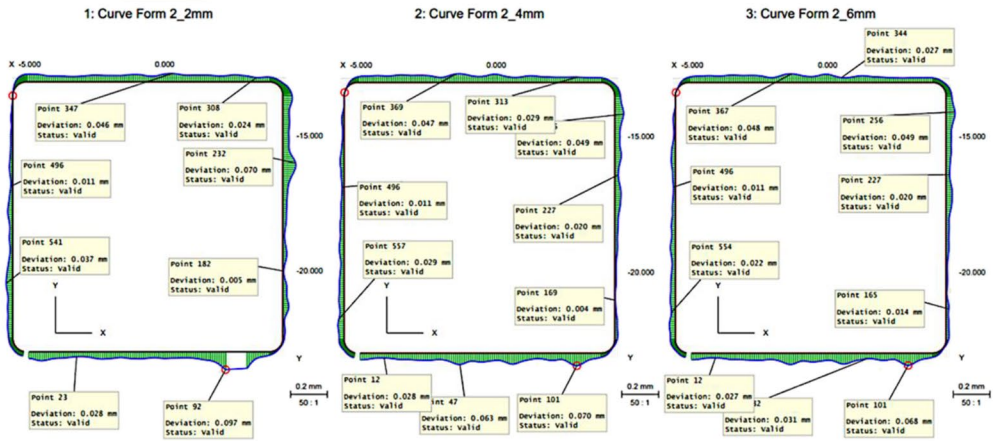

◂**Fig. 10** Geometry verifications on samples created using a double contour: the green areas represent the displacement of the real profile of the parts measured by the probe of the CMM machine from the CAD profile. Peaks are often present in one specific region, which is located on the surface that is opposite the gas flow and near the corner of the samples where the first contact with the blade occurs

to completion had generally the lower of the two velocities considered. In Fig. 13 are reported the *Sa* values obtained on the samples with and without contact-less supports, for each inclination angle. As can be seen, *Sa* is lower for the samples obtained with a down-skin velocity of 450 mm/s (lines with rounded marks in the graph). Moreover, it should be noted that all the samples have comparable *Sa* values for the 45° surfaces, probably because the down-facing surfaces are self-supporting for angles equal to or wider than 45°; thus, the effects of the supporting system are missed. The use of contactless supports helps reduce the down-skin roughness when the inclination angle is smaller, but the effectiveness of such supports is not so evident for the biggest gaps examined. The best results have been obtained for the supported samples with a gap of only 90 µm between the part and the support. If compared to the unsupported arcs, *Sa* of such samples is more or less reduced by 50%. No weld points were detected. On the contrary, a gap of 7 times the layer thickness was revealed to be inefficient for reducing the surface roughness but helped reduce the critical angle achieved anyway. A gap of 150 µm did not show improvements in terms of down-skin roughness, but also in this case, it helped further reduce the limiting angle, with respect to the unsupported parts.

Table 5 Average displacement from CAD model

Sample	Average displacement [mm]		
	2 mm	4 mm	6 mm
1	0.049	0.044	0.046
2	0.046	0.042	0.047
3	0.050	0.047	0.056
4	0.053	0.046	0.047
5	0.057	0.049	0.046
6	0.043	0.039	0.045
7	0.043	0.040	0.041
8	0.031	0.029	0.029
9	0.052	0.048	0.054
10	0.048	0.040	0.038

3.4 Superconducting radiofrequency cavities application

One of the most challenging applications of additively manufactured niobium is the production of superconducting radiofrequency (SRF) cavities to be used in particle accelerators. The main difficulties concerning this are the assurance of the purity of the material and the surface finish of the inner surfaces, which has to be excellent (absence of any defect on the surface, *Sa* lower than 1 µm, and mirror-like). These cavities are generally obtained by coupling two halves together and welding is done in the equatorial region of the component. However, the possibility that impurities and defects are introduced in the welded zone is highly likely, and the performances of the cavities would be greatly influenced. Thus, new manufacturing processes that allow the creation of seamless cavities are under investigation. Studies on additive manufacturing of SRF cavities are reported in the literature [27], but difficulties in obtaining one-piece cavities are stated since the most limiting factor is the extremely poor down-skin surface quality, which makes the as-built surface texture unacceptable for the final application. As mentioned above in this paper (see Section 1), the use of traditional supports is also deleterious. So, a one-piece 6 GHz SRF cavity was printed by using the contact-free support strategy. The upper half of the cavity is the most critical region because the inclination angle is just 18°. Using the contactless supporting system, the inner downward-facing surface was remarkably improved and the job went to completion successfully (Fig. 14a). Figure 14 shows the inner up-skin and down-skin of the cavity printed. As can be seen, the as-built surface finish is similar between the two regions. Thus, the efficacy of contactless supports was demonstrated. Due to the small dimensions of the object, it is not possible to

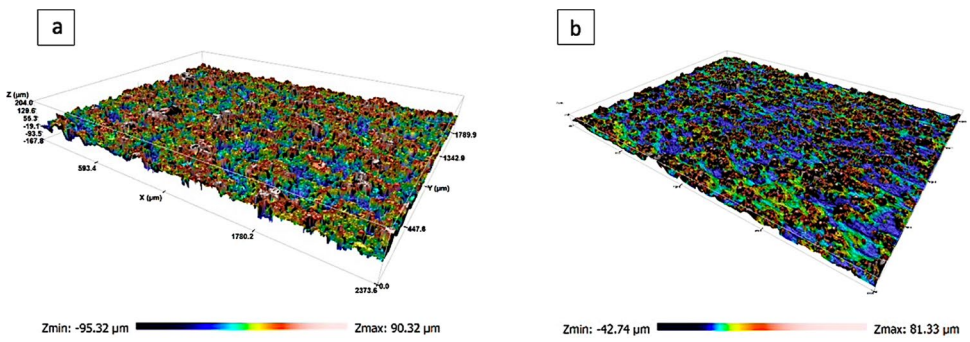

Fig. 11 Surface topology of the vertical faces of niobium cubic samples: **a** as-built surface finish without contour; **b** as-built surface finish with contour. The use of contour visibly increases the homogeneity of the surface texture

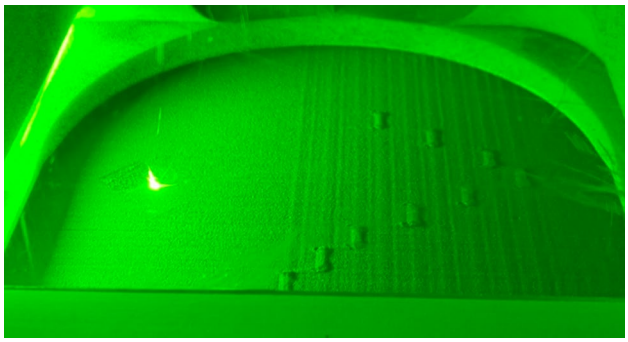

Fig. 12 Effects of the warpage of the parts on the powder layer: the recoater jumped on the down-skin edges (right side of the parts), which were higher than the rest of the section because of excessive energy input

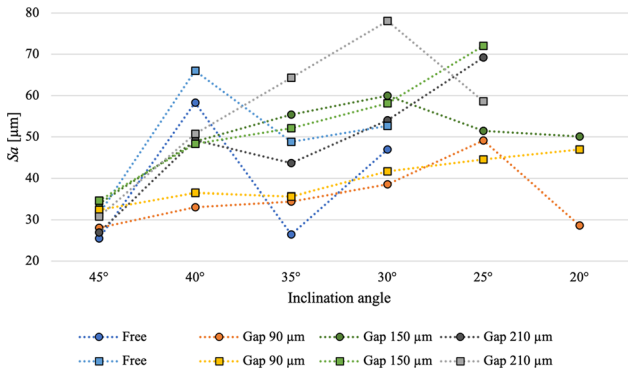

Fig. 13 *Sa* parameter computed on the down-skin areas of the arcs for each inclination angle (when possible). The gap of 90 µm seems to reduce consistently the down-skin surface roughness; parts produced setting a gap 90 µm wide went to completion, reaching the minimum overhang angle of 20° independently from the down-skin velocity employed

carry out surface roughness measurements without cutting the cavity. Further investigations on the part are ongoing to test its performance.

4 Conclusions

In this work, pure niobium was processed with Laser-Based Powder Bed Fusion additive manufacturing technique. Process parameters were optimized for achieving relative density higher than 99.5% and for reducing as much as possible the down-skin surface roughness. Density measurements were performed following the Archimedes principle. The maximum density obtained in this study is equal to 99.87%, while the surface roughness of several samples produced with different scanning strategies was evaluated by using an optical profilometer. The use of the contour helped reduce the as-built surface roughness by more than 50% for vertical walls, reaching a *Sa* of 10 µm. However, it was noticed that the contour was not homogeneous, especially on those sides of the samples that are opposite to the gas flow and the recoater direction some points of discontinuity were present. The causes of such defects are still unclear, so further investigations are needed to better understand the reasons for the discontinuity of the contour that was noticed in the experience reported in this paper.

The critical angle of the overhang surface was also investigated, revealing that angles smaller than 30° cannot be printed despite the down-skin parameters modifications. An innovative contactless supporting system was developed in order to reduce the self-supported limiting angle of pure niobium parts. The gap value between part and support was examined for preventing contact points or, in case of a too-wide space, undermining the possible beneficial effect of

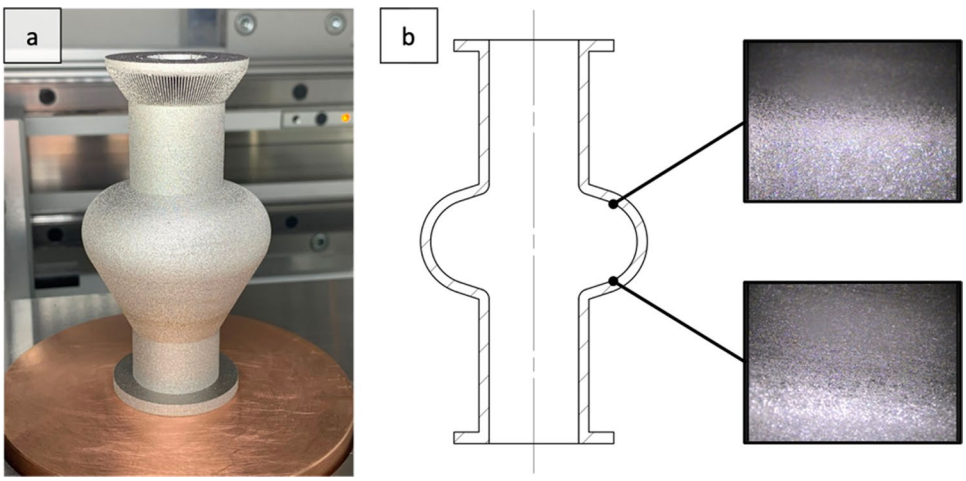

Fig. 14 Seamless 6 GHz cavity: **a** an entire cavity was successfully printed; **b** as-built conditions of the internal surface: from a visual inspection, the down-skin and the up-skin appear very similar; there are no dross formation and irregularities that typically characterize the down-skin surfaces

such a system, both in terms of heat dissipation and, as a consequence of this, minimum inclination angle. The effectiveness of such a contactless support strategy was demonstrated to produce down-facing angles lower than 30°, while the efficacy of the approach was not so evident for angles equal to or higher than 40°. The contact-free supports helped reduce the downward-facing surface angle to 20° (minimum value tested in this work) and, at the same time, improved noticeably the down-skin surface roughness (a decrease of *Sa* by more than 50% has been seen) because the heat dissipation was enhanced. A seamless 6 GHz superconducting radiofrequency cavity was also successfully produced, and the efficacy of this innovative supporting system was confirmed. In conclusion, these new unconventional supports can be applied whenever the quality of the downward-facing surfaces must be assured. In addition, the time requested for removing the support structures is drastically reduced, as well as the post-process steps for improving the surface quality of the final product.

Acknowledgements The authors would like to thank Taniobis GmbH (Goslar, Germany) for providing the powder employed for this work.

Author contribution The authors' contributions to the manuscript are as follows: Silvia Candela: conceptualization, investigation, data curation, writing—original draft; Pietro Rebesan: conceptualization, investigation, data curation, writing—review and editing; Diego De Bortoli: investigation, data curation; Simone Carmignato: resources, writing—review and editing, supervision; Filippo Zanini: resources, data curation, writing—review and editing, supervision; Valentina Candela: conceptualization, writing—review and editing; Razvan Dima: resources, supervision; Adriano Pepato: conceptualization, resources, supervision, funding acquisition; Markus Weinmann: resources; Paolo Bettini: supervision.

Funding Open access funding provided by Università degli Studi di Padova within the CRUI-CARE Agreement. This project has received funding from the European Union's Horizon 2020 Research and Innovation programme under Grant Agreement No 101004730. This work has been carried out within the framework of the EUROfusion Consortium, funded by the European Union via the Euratom Research and Training Programme (Grant Agreement No 101052200 — EUROfusion). Views and opinions expressed are however those of the author(s) only and do not necessarily reflect those of the European Union or the European Commission. Neither the European Union nor the European Commission can be held responsible for them.

Declarations

Competing interests The authors declare no competing interests.

References

1. Linner R, Trueman DL, Burt R (2014) Tantalum and niobium. In: Gunn G, Critical metals handbook, 1th edn. John Wiley & Sons, pp 361–384. https://mmsallaboutmetallurgy.com/wp-content/uploads/2019/07/Critical-Metals-Handbook.pdf. Accessed 3 Aug 2022
2. Schulz KJ, Piatak NM, Papp JF (2017) Niobium and tantalum. In: Schulz KJ, DeYoung JH Jr, Seal RR II, Bradley DC (eds) Critical mineral resources of the United States—economic and environmental geology and prospects for future supply. U.S. Geological Survey Professional Paper 1802, pp M1–M34. https://doi.org/10.3133/pp1802M
3. Grill R, Gnadenberger A (2006) Niobium as mint metal: production-properties-processing. Int J Refract Met H 24:275–282. https://doi.org/10.1016/j.ijrmhm.2005.10.008
4. Finnemore DK, Stromberg TF, Swenson CA (1966) Superconducting properties of high-purity niobium. Phys Rev 149(1):231–243. https://doi.org/10.1103/PhysRev.149.231
5. Lynton EA, Mclean WL (1967) Type II superconductors. Adv Electron El Phys 23:1–37. https://doi.org/10.1016/S0065-2539(08)60059-1
6. Padamsee H (2009) Surface resistance and critical filed. In: Padamse H, RF Superconductivity: science, technology, and applications. John Wiley & Sons, pp 41–83. https://doi.org/10.1002/9783527627172.ch3
7. Di Zenobio A, Albanese R, Anemona A, Biancolini ME, Bonifetto R, Brutti C, Corato V, Crisanti F, Della Corte A, De Marzi G, Fiamozzi Zignani C, Giorgetti F, Messina G, Muzzi L, Savoldi L, Tomassetti G, Turtù S, Villone F, Zappatore A (2017) DTT device: conceptual design of the superconducting magnet system. Fusion Eng Des 122:299–312. https://doi.org/10.1016/j.fusengdes.2017.03.102
8. Isono T, Koizumi N, Okuno K, Kurihara R, Nishio S, Tobita K, Demo Plant Design Team (2006) Design study of superconducting coils for the fusion DEMO plant at JAERI. Fusion Eng Des 81:1257–1261. https://doi.org/10.1016/j.fusengdes.2005.08.078
9. Satya Prasad VV, Baligidad RG, Gokhale AA (2017) Niobium and other high temperature refractory metals for aerospace applications. In: Aerospace materials and material technology. Indian Institute of Metals Series, pp 267–288. https://doi.org/10.1007/978-981-10-2134-3_12
10. Schulz K, Papp J (2014) Niobium and tantalum: indispensable twins. Fact Sheet US Geological Survey 2014-3054 https://doi.org/10.3133/fs20143054
11. Griemsmann T, Abel A, Hoff C, Hermsdorf J, Weinmann M, Kaierle S (2021) Laser-based powder bed fusion of niobium with different build-up rates. Int J Adv Manuf Technol 114:305–317. https://doi.org/10.1007/s00170-021-06645-y
12. Fox JC, Moylan SP, Lane BM (2016) Effect of process parameters on the surface roughness of overhanging structures in laser powder bed fusion additive manufacturing. 3rd CIRP Conference on Surface Integrity. Procedia CIRP 45:131–134. https://doi.org/10.1016/j.procir.2016.02.347
13. Çelik A, Tekoğlu E, Yasa E, Sönmez MŞ (2022) Contact-free support structures for the direct metal laser melting process. Materials 15:3765. https://doi.org/10.3390/ma15113765
14. Vandenbroucke B, Kruth JP (2007) Selective laser melting of biocompatible metals for rapid manufacturing of medical parts.

Rapid Prototyping J 13(4):196–203. https://doi.org/10.1108/13552540710776142
15. Pérez M, Garcìa-Collado A, Carou D, Medina-Sànchez G, Dorado-Vicente R (2021) On surface quality of engineered parts manufactured by additive manufacturing and postfinisching by machining. In: Pou J, Riveiro A, Davim JP (eds) Additive Manufacturing. Elsevier, pp 369–394. https://doi.org/10.1016/B978-0-12-818411-0.00015-X
16. Strano G, Hao L, Everson R M, Evans K E (2013) Surface roughness analysis, modelling and prediction in selective laser melting. J Mater Process Tech 213 589-597 https://doi.org/10.1016/j.jmatprotec.2012.11.011
17. Vitale V, Stravdiris J, Salmi A, Bonndioli F, Saboori A (2022) Optimization of downskin parameters to produce metallic parts via laser powder bed fusion process: an overview. Int J Adv Manuf Technol 123:2159–2182. https://doi.org/10.1007/s00170-022-10314-z
18. Candela V, Pozzi M, Chyhyrynets E, Garcia Diaz V, Candela S, Dima R, Favero G, Pira C, Pepato A, Sonato P (2022) Smoothening of the down-skin regions of copper components produced via Laser Powder Bed Fusion Technology. Int J Adv Manuf Technol 123:3205–3221. https://doi.org/10.1007/s00170-022-10408-8
19. Paggi U, Thijs L, Van Horeweder B (2022) Implementation of contactless supports for industrially relevant additively manufactured parts in metal. Addit Manuf Lett 3:100095. https://doi.org/10.1016/j.addlet.2022.100095
20. AMtrinsic® Spherical Nb powder for Additive Manufacturing. https://www.taniobis.com/settings/file/85a37c136d638b02016da69c39921512.de.0/flyer%20nb_taniobis_11_2022.pdf. Accessed 1 Feb 2022
21. Rebesan P, Gennari C, Zorzi F, Bonesso M, Calliari I, Dima R, Pepato A, Vedani M (2021) Interface analysis of additively manufactured pure molybdenum and AISI 304 stainless steel building-plate. Mater Lett 305:130763. https://doi.org/10.1016/j.matlet.2021.130763
22. Hajitabar A, Naffakh-Moosavy H (2017) Electron beam welding of difficult-to-weld austenitic stainless steel/Nb-based alloy dissimilar joints without interlayer. Vacuum 146:170–178. https://doi.org/10.1007/s00170-022-10408-8
23. Guoqing C, Binggang Z, Yuan Z, Binghui D, Jicai F (2013) Microstructure and properties of electron beam welded tantalum-to-stainless steel joints. Rare Metal Mat Eng 42(5):0914–0918. https://doi.org/10.1016/S1875-5372(13)60067-3
24. Mettler Toledo ME User Manual. https://www.mt.com/ch/it/home/library/product-brochures/laboratory-weighing/basic_weighing/LabTec_OI_ME.html?cmp=als_me-rm. Accessed 7 Jun 2022
25. ISO 25178-2 (2021) Geometrical product specifications (GPS) – surface texture: areal – part 2: terms, definitions and surface texture parameters. ISO, Geneve
26. Scipioni Bertoli U, Wolfer AJ, Matthews MJ, Delplanque JPR, Schoenung JM (2017) On the limitations of Volumetric Energy Density as a design parameter for Selective Laser Melting. Mater Des 113:331–340. https://doi.org/10.1016/j.matdes.2016.10.037
27. Terrazas CA, Mireles J, Gaytan SM, Morton PA, Hinojos A, Frigola P, Wicker RB (2016) Fabrication and characterization of high-purity niobium using electron beam melting additive manufacturing technology. Int J Adv Manuf Technol 84:1115–1126. https://doi.org/10.1007/s00170-015-7767-x